Layer KKR approach to Bloch-wave transmission and reflection: Application to spin-dependent tunneling

J. M. MacLaren

Department of Physics, Tulane University, New Orleans, Louisiana 70118

X.-G. Zhang

Computational Physics and Engineering Division, Oak Ridge National Laboratory, P.O. Box 2008, Oak Ridge, Tennessee 37831-6114

W. H. Butler and Xindong Wang

Metals and Ceramics Division, Oak Ridge National Laboratory, P.O. Box 2008, Oak Ridge, Tennessee 37831-6114

Bloch waves may be reflected and transmitted by planar interfaces. In this paper, we show how the reflection and transmission amplitudes for Bloch waves can be calculated within the layer Korringa-Kohn-Rostoker formalism. The calculated transmission probability is used to calculate the spin-dependent tunneling conductance for magnetic tunnel junctions formed from ZnSe semiconducting layers sandwiched between two ferromagnetic Fe layers. [S0163-1829(99)01308-9]

I. INTRODUCTION

When Bloch electrons encounter planar interfaces they may be reflected and/or transmitted.[1] In this paper, we develop techniques for calculating these reflection and transmission amplitudes within the layer Korringa-Kohn-Rostoker (LKKR) approach,[2] a technique for first-principles electronic structure calculations. The LKKR technique is particularly well adapted to layered systems because the computation time scales linearly in the number of different atomic layers. An additional advantage of the LKKR technique is that it does not require periodicity in the direction perpendicular to the layers. However, it does require that the two-dimensional Bravais lattice be the same for all atomic layers. The LKKR is also well adapted to calculating reflection and transmission amplitudes. In fact, the LKKR procedure works by calculating scattering matrices for each atomic layer in a partial wave representation, converting to a plane-wave basis and then propagating these plane waves through the system by means of transmission and reflection amplitudes.

There are many uses for Bloch wave transmission and reflection amplitudes and probabilities. They can be used, for example, to generalize the free-electron theory of transport in films and metallic multilayer[3,4] so that it can be applied to real materials.[5] They can also be used to develop a first-principles based theory of electron tunneling. We shall use the latter application in this paper as an illustration of the utility of the Bloch wave transmission and reflection amplitudes, and as a demonstration of our ability to calculate them for relatively large systems using the LKKR technique.

The ability to calculate Bloch wave transmission and reflection amplitudes for general materials including transition metals and for relatively large systems allows us to investigate new effects such as the spin-dependent tunneling effect[6–10] in which the tunneling current between two ferromagnetic electrodes separated by an insulator or semiconductor depends upon the relative orientation of the magnetic moments in the electrodes. This effect has elicited considerable interest recently because it may be applied to make devices that can sense magnetic fields. Application of the effect to information storage and retrieval devices is being investigated in several laboratories.

In Sec. II, we describe how the LKKR can be used to calculate Bloch states and their group velocities. In Sec. III, we show how to transform from the transmission and reflection amplitudes of plane waves that the LKKR generates in solving the the electronic structure problem to the transmission and reflection amplitudes of the Bloch waves. In Sec. IV, we use the Landauer conductance formula to evaluate the tunneling conductance for a sandwich structure consisting of a (100) layer of ZnSe (of various thicknesses) sandwiched between Fe (100) electrodes.

II. LKKR THEORY OF BLOCH STATES AND GROUP VELOCITIES

In this section, we shall briefly describe the LKKR method for computing the self-consistent electronic structure of an interface. Since the details have already been published elsewhere, only a brief summary of the approach relevant to computing the tunneling conductance will be given. After this brief introduction, a method for calculating the Bloch states and the z component of the Bloch wave group velocity will be presented. Finally, the derivation of the unitary scattering S matrix describing the scattering of the Bloch states by the interface will be given.

A. The self-consistent solution

The LKKR method is a self-consistent electronic structure method, based upon the local spin-density approximation, or some other approximation to density-functional theory, which can evaluate the electronic structure of a three-dimensional solid without requiring the usual constraint of three-dimensional translational symmetry. The extended

solid is viewed as one composed of an infinite stack of planes of atoms, each of which has two-dimensional translational symmetry. Thus, the method is ideally suited to the problem at hand, namely a system formed of two semi-infinite stacks of layers, which form the leads, on either side of the tunnel barrier. Magnetism is treated within the local spin-density approximation, in which the spin-up and spin-down densities are allowed to converge independently. In this paper, the Perdew Zunger parametrized form of exchange-correlation potential was used.[11] This approximation fits the correlation energy for paramagnetic, and a fully spin polarized, homogeneous electron gas obtained from Monte Carlo simulations performed by Ceperley and Alder.[12] Values for intermediate spin polarizations were obtained from an interpolation formula derived by Vosko et al.[13]

The calculation for an interface proceeds as follows, first, a bulk calculation is performed to find the self-consistent potentials for the two leads on layers far from the sample. Since in a metallic system screening ensures that the electronic perturbations in the leads, due to the tunnel junction, will be localized spatially at the interface, atoms far from the barrier are assumed to have bulklike potentials whose values are those obtained from the corresponding bulk calculation.

Then an interface containing the sample is set up, and the spin-up and spin-down potentials on atomic layers within the sample and within the leads near the interface are allowed to relax through the iterative procedure described above until electrostatic self-consistency is achieved throughout the system. We find that the self-consistently calculated potentials seldom differ significantly from those of the bulk if they are more than three or four layers from the interface. A detailed description of the self-consistent calculation of interfacial electronic structures, which allows for layer-dependent magnetism, can be found in previous publications,[2,14,15] to which we refer the reader. A self-consistent charge and spin density is found in this manner.

B. Computation of Bloch states and Bloch velocities

The Bloch states are derived from a transfer-matrix analysis. The approach is a straight-forward generalization of a one-dimensional (1D) theory. In essence, those planes of atoms, which when repeated form the bulk periodic lead, are grouped into a single layer. Between each layer the ith Bloch wave is expanded in terms of plane waves.

$$\phi_i = \sum_{\mathbf{g}} c_{\mathbf{g}}^{i+} \exp(i\mathbf{K}_{\mathbf{g}}^+ \cdot \mathbf{r}) + \sum_{\mathbf{g}} c_{\mathbf{g}}^{i-} \exp(i\mathbf{K}_{\mathbf{g}}^- \cdot \mathbf{r}). \quad (2.1)$$

The wave vectors $\mathbf{K}_{\mathbf{g}}^\pm$, in the plane waves $\exp(i\mathbf{K}_{\mathbf{g}}^\pm \cdot \mathbf{r})$, are given by

$$\mathbf{K}_{\mathbf{g}}^\pm = \left\{ \mathbf{k}_\parallel + \mathbf{g}, \pm \sqrt{\frac{2m}{\hbar^2}E - (\mathbf{k}_\parallel + \mathbf{g})^2} \right\}, \quad (2.2)$$

where the vectors $\mathbf{g}$ are two-dimensional reciprocal lattice vectors and $\mathbf{k}_\parallel$ is a wave vector in the first two-dimensional Brillouin zone. Each layer is characterized, in the plane wave representation, by four scattering matrices, $t_{\mathbf{gg}'}^{++}$, $t_{\mathbf{gg}'}^{+-}$, $t_{\mathbf{gg}'}^{-+}$, and $t_{\mathbf{gg}'}^{--}$. Expressions for these matrices can be found in Ref.

2. The superscripts refer to the direction of travel of incident and outgoing plane waves, respectively.

The connection between the Bloch wave amplitudes between adjacent layers is given by

$$(c^{i+} c^{i-}) \begin{pmatrix} t^{++} & -t^{+-} \\ 0 & 1 \end{pmatrix} = \exp(i\mathbf{k} \cdot \mathbf{R})(c^{i+} c^{i-})$$

$$\times \begin{pmatrix} 1 & 0 \\ -t^{-+} & t^{--} \end{pmatrix}. \quad (2.3)$$

$\mathbf{R}$ is the repeat vector between the identical layers forming the bulk crystal and $\mathbf{k} = (\mathbf{k}_\parallel, k_z)$. These equations represent a generalized eigenvalue problem which can be solved using standard numerical routines such as those obtainable from LAPACK.[16] By specifying values of $\mathbf{k}_\parallel$ and the energy E, taken to be the Fermi energy in this application, we can solve for the eigenvalues k_z and the corresponding eigenvectors. Usually only a few values of k_z are found to be real; these correspond to the Bloch states.

In addition to the band structure, it is essential to compute the z component of the group velocity so that the direction of travel of each Bloch state can be determined, and consequently whether the state belongs to the subspace of incident or scattered channels. We have found a simple way of extracting this from the band structure without needing to resort to numerical differentiation. The z component of the group velocity is found by noting that the eigenvalue $E(\mathbf{k})$ is an analytic function of the wave vector $\mathbf{k}$. Thus, if a small imaginary part ΔE is given to the energy, the calculated value of k_z will also have a small imaginary part Δk_z. The two are related by the velocity,

$$v_z = \frac{1}{\hbar} \frac{\partial E}{\partial k_z} \approx \frac{1}{\hbar} \frac{\Delta E}{\Delta k_z}. \quad (2.4)$$

The real part of k_z will be left unaltered, hence both k_z and v_z can be found simultaneously.

Because E is a periodic function of k_z, it follows that for a given value of $\mathbf{k}_\parallel$ there will be exactly as many states with positive v_z as with negative. The z component of the Bloch state's group velocity determines its direction of travel. Note that this is different from $\hbar k_z/m$. It is quite common to have a Fermi surface for which (for given $\mathbf{k}_\parallel$) there are two or four values of k_z that are greater than zero and none that are less than zero. If k_z were used to determine the direction of the Bloch wave's travel one would have the unphysical result that electrons with that value of $\mathbf{k}_\parallel$ could only propagate in one direction.

Since the two leads may be different, calculations of the Bloch states are done for both the left- and the right-hand sides of the barrier. Each Bloch state at the Fermi energy corresponds to a channel in the Landauer-Büttiker formalism. Those states traveling towards the barrier correspond to incident channels while those traveling away from the barrier correspond to the scattered (transmitted or reflected) channels. These two subspaces will be used to define the scattering S matrix.

III. SCATTERING THEORY FOR BLOCH WAVES

In this section, we shall show how the reflection and transmission coefficients for Bloch waves incident on the sample from one of the leads may be calculated from the plane-wave reflection and transmission coefficients ($t_{gg'}^{++}$, $t_{gg'}^{--}$, $t_{gg'}^{+-}$, $t_{gg'}^{-+}$) that are generated by the layer KKR method. We consider here systems that have two-dimensional periodicity so that momentum parallel to the interface is conserved. Our procedures have some similarities to the techniques developed by Stiles and Hamann[17,18] to calculate the transmission of Bloch waves through interfaces, that used a variational procedure of Wachutka and Bross[19,20] to join wave functions on opposite sides of an interface. After this paper was submitted for publication, but before it was accepted, we learned of the recent work of van Hoof[21] who calculated transmission probabilities using an embedding method developed by Inglesfield.[22]

It is convenient to label the Bloch wave functions for the bulk material that makes up the leads by a two-dimensional wave vector $\mathbf{k}_\parallel$, and the value of the z component of the wave vector k_z. Since the z component of the group velocity has also been computed, these k_z values will be labeled with superscript $+$ or $-$ to indicate the direction of travel, i.e., whether v_z is greater than zero or less than zero. For clarity of notation, all of the subsequent formulas assume a fixed $\mathbf{k}_\parallel$. Using this modified notation, Eq. (2.1) can be rewritten as

$$\phi_{k_z^\pm} = \sum_{\mathbf{g}} c_{k_z^\pm \mathbf{g}}^+ \exp(i\mathbf{K_g^+}\cdot\mathbf{r}) + \sum_{\mathbf{g}} c_{k_z^\pm \mathbf{g}}^- \exp(i\mathbf{K_g^-}\cdot\mathbf{r}),$$
(3.1)

where the sum runs over the N_g reciprocal lattice vectors that are needed to accurately represent the wave function. Conversely, a plane wave can be expanded in terms of the Bloch wave functions, $\phi_{k_z}(\mathbf{r})$,

$$e^{i\mathbf{K_g^\pm}\cdot\mathbf{r}} = \sum_{k_z^+} \mu_{\mathbf{g}k_z^+}^\pm \phi_{k_z^+}(\mathbf{r}) + \sum_{k_z^-} \mu_{\mathbf{g}k_z^-}^\pm \phi_{k_z^-}(\mathbf{r}).$$
(3.2)

Note that this expansion includes all of the eigenvectors that are solutions to Eq. (2.3), not just those eigenfunctions that correspond to traveling Bloch waves (i.e., those with real values of k_z). The expansion coefficients, μ, can be found from the inverse of the matrix of eigenvector coefficients c.

We can expand the total wave function on the left-hand side of the barrier due to an incident wave plane wave with wavevector $\mathbf{K_g^+}$, in terms of Bloch waves and obtain

$$\psi_{\mathbf{g}}^{L+} = \sum_{k_z^+} A_{\mathbf{g}+k_z^+}^L \phi_{k_z^+}^L(\mathbf{r}) + \sum_{k_z^-} A_{\mathbf{g}+k_z^-}^L \phi_{k_z^-}^L(\mathbf{r})$$

$$= e^{i\mathbf{K_g^+}\cdot\mathbf{r}} + \sum_{\mathbf{g}'} t_{\mathbf{g}\mathbf{g}'}^{+-} e^{i\mathbf{K_{g'}^-}\cdot\mathbf{r}},$$
(3.3)

where

$$A_{\mathbf{g}+k_z^\pm}^L = \mu_{\mathbf{g}k_z^\pm}^{L+} + \sum_{\mathbf{g}'} t_{\mathbf{g}\mathbf{g}'}^{+-} \mu_{\mathbf{g}'k_z^\pm}^{L-}.$$
(3.4)

To the right of the sample we have

$$\psi_{\mathbf{g}}^{R+} = \sum_{k_z^+} A_{\mathbf{g}+k_z^+}^R \phi_{k_z^+}^R(\mathbf{r}) + \sum_{k_z^-} A_{\mathbf{g}+k_z^-}^R \phi_{k_z^-}^R(\mathbf{r})$$

$$= \sum_{\mathbf{g}'} t_{\mathbf{g}\mathbf{g}'}^{++} e^{i\mathbf{K_{g'}^+}\cdot\mathbf{r}},$$
(3.5)

with

$$A_{\mathbf{g}+k_z^\pm}^R = \sum_{\mathbf{g}'} t_{\mathbf{g}\mathbf{g}'}^{++} \mu_{\mathbf{g}'k_z^\pm}^{R+}.$$
(3.6)

A similar calculation can be performed for an incident plane wave from the right. The formulas for the coefficients $A_{\mathbf{g}-k_z^\pm}^R A_{\mathbf{g}-k_z^\pm}^L$ can be simply obtained by swapping the superscripts L and R and ''+'' and ''−'' on the plane-wave labels, i.e.,

$$A_{\mathbf{g}-k_z^\pm}^L = \sum_{\mathbf{g}'} t_{\mathbf{g}\mathbf{g}'}^{--} \mu_{\mathbf{g}'k_z^\pm}^{L-},$$
(3.7)

$$A_{\mathbf{g}-k_z^\pm}^R = \mu_{\mathbf{g}k_z^\pm}^{R-} + \sum_{\mathbf{g}'} t_{\mathbf{g}\mathbf{g}'}^{-+} \mu_{\mathbf{g}'k_z^\pm}^{R+}.$$
(3.8)

We have used superscripts L and R to allow for the the possibility that the leads on the left and on the right may have different Bloch states. This superscript is also used to imply appropriate values of $k_z^\pm$, since these too may be different in each lead.

If we now view the whole process as scattering of the Bloch waves, then the amplitude of the outgoing Bloch wave on the left side of the sample $A_{k_z^-}^L$ will be the sum of the transmitted Bloch waves from the right $A_{k_z^-}^R T^{--}$ and the reflected part of Bloch waves incident from the left $A_{k_z^+}^L T^{+-}$. Thus, $A_{\mathbf{g}\pm k_z^-}^L$ is given by

$$A_{\mathbf{g}\pm k_z^-}^L = \sum_{k_z'^+} A_{\mathbf{g}\pm k_z'^+}^L T_{k_z'^+ k_z^-}^{+-} + \sum_{k_z'^-} A_{\mathbf{g}\pm k_z'^-}^R T_{k_z'^- k_z^-}^{--}, \quad (3.9)$$

where $T_{k_z'^+ k_z^-}^{+-}$ and $T_{k_z'^- k_z^-}^{--}$ are the reflection coefficients for Bloch waves incident from the left, and the transmission coefficients for Bloch waves incident from the right, respectively. The right traveling Bloch waves on the right side of the sample are also a sum of reflected and transmitted Bloch waves

$$A_{\mathbf{g}\pm k_z^+}^R = \sum_{k_z'^+} A_{\mathbf{g}\pm k_z'^+}^L T_{k_z'^+ k_z^+}^{++} + \sum_{k_z'^-} A_{\mathbf{g}\pm k_z'^-}^R T_{k_z'^- k_z^+}^{-+}.$$
(3.10)

$T_{k_z'^+ k_z^+}^{++}$ and $T_{k_z'^- k_z^+}^{-+}$ are the transmission coefficients for Bloch waves incident from the left-hand side of the barrier, and reflection coefficients for Bloch waves incident from the right-hand side of the barrier.

The four equations represented by [Eqs. (3.9) and (3.10)] can be combined into a matrix form,

$$\begin{pmatrix} A^{L}_{\mathbf{g}^{+}k_{z}^{+}} & A^{R}_{\mathbf{g}^{+}k_{z}^{-}} \\ A^{L}_{\mathbf{g}^{-}k_{z}^{+}} & A^{R}_{\mathbf{g}^{-}k_{z}^{-}} \end{pmatrix} S = \begin{pmatrix} A^{R}_{\mathbf{g}^{+}k_{z}^{+}} & A^{L}_{\mathbf{g}^{+}k_{z}^{-}} \\ A^{R}_{\mathbf{g}^{-}k_{z}^{+}} & A^{L}_{\mathbf{g}^{-}k_{z}^{-}} \end{pmatrix}, \quad (3.11)$$

where the S matrix is defined as

$$S = \begin{pmatrix} T^{++} & T^{+-} \\ T^{-+} & T^{--} \end{pmatrix}, \qquad (3.12)$$

which can then be solved for T^{++}, T^{+-}, T^{-+}, and T^{--} in terms of the coefficients $A^{L,R}_{\mathbf{g}^{\pm}k_{z}^{\pm}}$. This formalism is not equivalent to a simple unitary transformation of the S matrix in a plane-wave basis since each Bloch state contains plane waves traveling in both directions, or, equivalently a single plane wave is composed of Bloch states traveling in both directions.

The S matrix of Eq. (3.11) has dimensions $2N_{g} \times 2N_{g}$. The submatrix of S formed on the subspace of traveling Bloch states (S_{t}) is unitary ($S_{t}S_{t}^{\dagger} = I$), provided the traveling Bloch states are normalized to unit flux. In computing the flux of each Bloch state, the plane-wave basis set is used, and care must be taken to count correctly the contribution from both traveling and evanescent plane waves, since the expansion coefficients of the Bloch states are in general complex.

IV. CALCULATION OF THE TUNNELING CONDUCTANCE

We have applied this technique to calculate the conductance of a tunnel junction formed from several [100] layers of ZnSe sandwiched between two semi-infinite stacks of Fe [100] layers, which form the ''leads.'' Systems of this type are interesting because it can be arranged that the moments of the two Fe layers are aligned antiparallel in the absence of an external magnetic field. The application of a small magnetic field may then cause alignment of the moments which in turn causes a significant change in the tunneling conductance.

The structure of the interface between the bcc Fe and the zinc-blende ZnSe structures is shown in Fig. 1. The usual cubic cells for bcc and zinc blende are rotated by 45° relative to each other. The reader is asked to imagine that the atomic planes extend to infinity in the directions parallel to the planes and that the iron layers are repeated indefinitely to the left and to the right. The figure does not distinguish between the Zn and Se atoms, which occupy alternate atomic planes of the interlayer. It was assumed that Zn layers are adjacent to the Fe electrodes.

The lattice mismatch between Fe [100] and several diamond and zinc-blende semiconductors is quite small. The lattice constant for bcc Fe is 2.87 Å, while those of Ge, GaAs, and ZnSe are 5.66, 5.65, and 5.67 Å , respectively. The lattice constants of the semiconductors are almost ex-
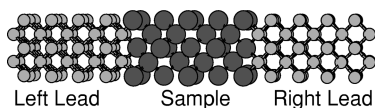
FIG. 2. Charges redistribute when ZnSe is embedded in Fe. Here it is assumed that the Zn layers are adjacent to the Fe.

actly twice that of Fe, leading to modest lattice mismatches of only about 1.4%. We chose to study ZnSe as the barrier layer since it has been suggested that this may be the easiest of the three possible semiconductor systems to grow epitaxially as an interlayer between Fe electrodes. The lattice constant of the whole system was fixed to that for bulk bcc Fe, causing a slight isotropic expansion of all the ZnSe layers.

The calculation proceeded by first calculating self-consistently the electronic structure for a periodic stack of [100] Fe layers using the local spin density to density-functional theory. The potentials generated were used both to compute the Bloch waves and to embed the Fe/ZnSe/Fe interface. The atomic sphere, rather than the muffin tin, approximation was adopted for both the potential and charge density. In the interface calculations, the potentials on four atomic layers of Fe on either side of the ZnSe, and all of the ZnSe layers were relaxed. The resulting redistribution of charges is shown in Fig. 2.

A dipole layer forms at the Fe/ZnSe interface as electrons are transferred from the Fe to the ZnSe in order to correctly position the Fermi energies of Fe and ZnSe. There is also charge transfer within the ZnSe as electrons are transferred from Se to Zn layers. Several calculations were performed using between 5 and 33 atomic layers of Zn and Se. For the sandwiches with more than 9 atomic layers of Zn and Se, the interior ZnSe potentials were not relaxed, but rather frozen at values corresponding to the innermost ZnSe self-consistent potentials calculated with 9 atomic layers of Zn and Se. The present calculations neglect spin-orbit coupling, spin-flip scattering and effects such as the spontaneous Hall effect that might arise from the self-field of the iron electrodes.

A preliminary description of the assumed physical structure and of the calculated electronic structure has already been published,[23] and so the results of that work will not be repeated here. In summary, these calculations showed that a significant density of states persists in the interior ZnSe layers at the Fermi energy, especially for the minority channel. A large peak in the minority density of states is found at the Fermi energy. The state is localized on the atoms close to the interface and corresponds to an interface resonance, which couples only weakly to the bulk Bloch states in the Fe leads. This feature is present for different semiconducting barriers,

FIG. 1. The system consists of a sample sandwiched between two semi-infinite leads. The system is assumed to be periodic in the directions parallel to the interfaces.
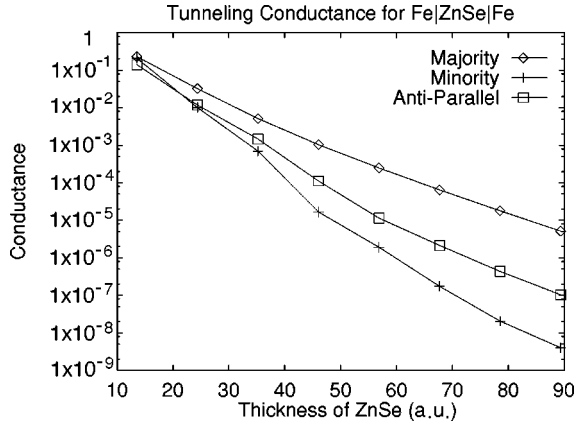
FIG. 3. Tunneling conductance for majority and minority spin channels for the case of aligned moments in the iron layers and tunneling conductance for one of the spin channels for the case of antiferromagnetic alignment of the spin channels. The conductance is in units of e^2/h per two-dimensional unit cell.

and is a consequence of the interface between a barrier and the Fe atoms. The impact of this state on the minority tunneling current will be discussed in this paper.

We note that the barrier is not a classical barrier since the electron kinetic energy exceeds the potential energy in the semiconductor with the exception of a few positions. Rather the barrier is formed as a result of interference, which precludes propagating states at certain energies. In order to make contact with traditional treatments of tunneling, which envision the semiconducting region as a simple barrier with parameters determined by the band gap in the bulk electronic structure, we used the potentials calculated for the central Zn and Se atomic layers to calculate the electronic structure of bulk ZnSe. We found that it has a direct gap at the zone center of 1.34 eV. The Fermi energy for the sandwich lies 0.49 eV above the valence band and 0.85 eV below the conduction band. In this traditional picture the semiconductor would be represented by a step barrier whose height is 0.85 eV. We would like to point out that the calculated band gap is only about half of the measured gap. It is well known that the local-density approximation to density-functional theory yields gaps that are too small for semiconducting systems. Although there are simple techniques that could be used to empirically adjust the bands to give the correct gap and Fermi-energy placement we prefer to present our initial results without adjustments.

We calculated the tunneling conductance for this Fe/ZnSe/Fe sandwich composed of (100) planes as a function of the thickness of the ZnSe interlayer for majority and minority channels and for parallel and antiparallel alignment of the moments in the two Fe layers. The conductance was calculated from the transmission probability $T(k_\parallel)$ using the relation[24]

$$G = \frac{e^2}{h} \sum_{k_\parallel} T(k_\parallel). \qquad (4.1)$$

This result can also be obtained from the Landauer-Büttiker formula for the conductance.[25–27]

The results, which are plotted in Fig. 3, show that the conductance is approximately an exponential function $e^{-d/l}$
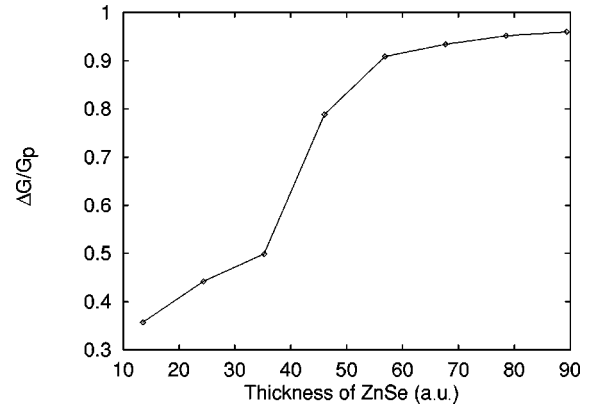
FIG. 4. Magnetoresistance as a function of ZnSe thickness for Fe/ZnSe/Fe sandwich.

of the barrier thickness d with a length of decay l that varies from approximately 4.6 Å for the majority electrons to approximately 3.7 Å for the minority electrons. Using the decay length for the majority electrons gives an effective barrier height, $\Delta V = \hbar^2/8m^*l^2$, of 0.045 eV if m^* is assumed to be the free-electron mass. Although this is small compared to the energy difference between the Fermi energy and the bottom of the conduction band in the ZnSe layers, the effective barrier height would be reasonable if the smaller effective mass of ZnSe were used in the estimation, as would be the case for states at the bottom of the conduction band in ZnSe. We have performed additional calculations[28] in which the barrier was a constant repulsive potential. For such a repulsive spatially constant barrier we found that $\hbar^2/8ml^2$ was almost exactly equal to the energy difference between the Fermi energy and the bottom of the conduction band in the barrier.

Figure 3 shows the variation in the tunneling current with thickness for minority and majority spin channels for ferromagnetic alignment of the Fe layers as well as that obtained when the two Fe layers are aligned antiferromagnetically. The thickness dependences of the majority channel conductance, of the minority channel conductance, and of the the tunneling conductance for either spin channel for the case of antiparallel alignment are significantly different. The more rapid decrease in the minority and antiparallel conductance compared to the majority leads to a tunneling conductance at large thicknesses that is dominated by the majority electrons. This yields a magnetoresistance ratio that approaches unity as shown in Fig. 4. This behavior is quite different from that observed in calculations that we performed in which the barrier was a constant potential.[28] For the case of a spatially constant barrier, the current in all channels decreases exponentially with thickness at the same rate so that the magnetoresistance ratio is independent of thickness, a result consistent with Slonczewski's[29] model calculations.

The tunneling currents as a function of $k_\parallel$ also vary considerably with spin channel and moment alignment as is shown in Figs. 5 and 6. For all thicknesses, the majority spin current is peaked near the center of the two-dimensional zone while for thin semiconducting interlayers (Fig. 5), the minority spin current has peaks that seem to form part of a circle centered at the origin of the zone. This structure corresponds precisely to the localized resonance states seen at

(a)   Majority Conductance for Parallel Alignment   (b)   Minority Conductance for Parallel Alignment

(c)   Conductance for Anti-Parallel Alignment
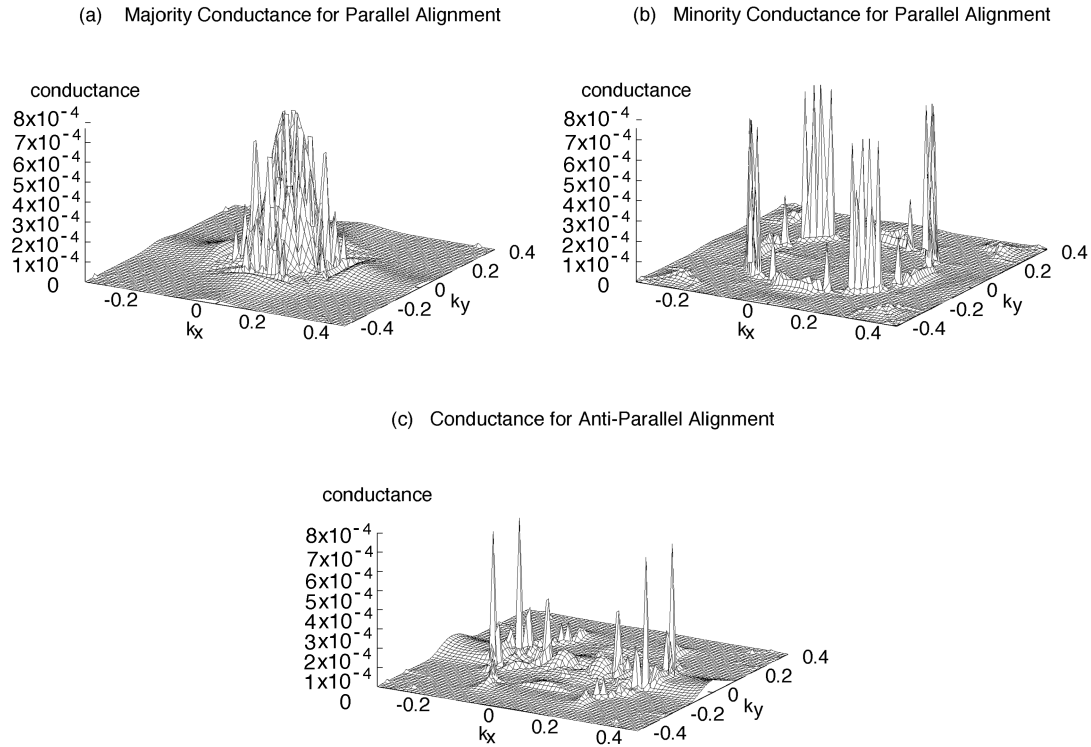
FIG. 5. Tunneling conductance through 20-a.u.-thick ZnSe barrier as a function of $\mathbf{k}_\parallel$ in the two-dimensional Brillouin zone for (a) majority spin channel (moments aligned), (b) minority spin channel (moments aligned), (c) conductance for either channel for antiparallel alignment of the moments. Conductance per two-dimensional cell is expressed in units of e^2/h. The two-dimensional cell contains two iron atoms or one atom of either Zn or Se.

(a)   Majority Conductance for Parallel Alignment   (b)   Minority Conductance for Parallel Alignment

(c)   Conductance for Anti-Parallel Alignment
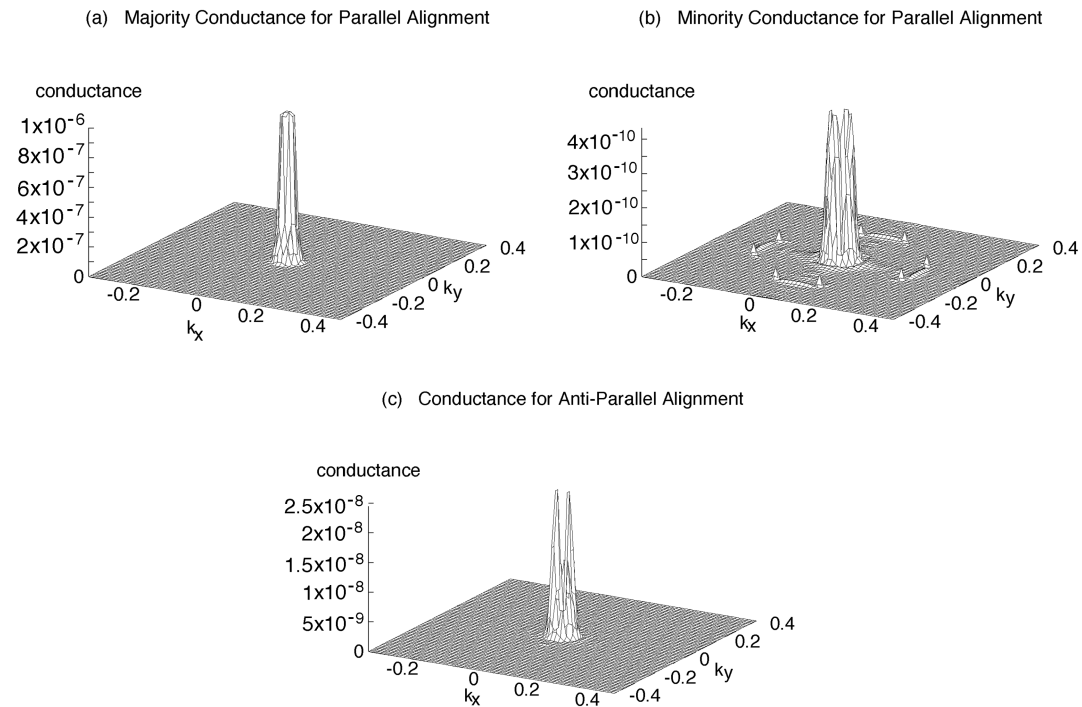
FIG. 6. Tunneling conductance through 90-a.u.-thick ZnSe barrier as a function of $\mathbf{k}_\parallel$ in the two-dimensional Brillouin zone for (a) majority spin channel (moments aligned), (b) minority spin channel (moments aligned), (c) conductance of either spin channel for antiparallel alignment of the moments. Conductance per two-dimensional cell is expressed in units of e^2/h. The two-dimensional cell contains two iron atoms or one atom of either Zn or Se.
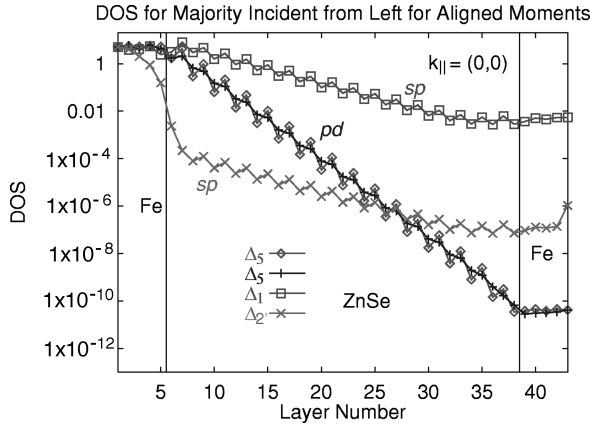
FIG. 7. Density of states for each of the majority Bloch states at $k_\parallel = 0$, for parallel alignment of the Fe moments.

FIG. 8. Density of states for each of the minority Bloch states at $k_\parallel = 0$, for parallel alignment of the Fe moments.

the interface in the minority spin channel. As the semiconducting layer becomes thicker (Fig. 6), the currents at larger values of $\mathbf{k}_\parallel$ are suppressed and the current *near* $\mathbf{k}_\parallel = 0$ becomes relatively larger, but the point $\mathbf{k}_\parallel = 0$ remains a local minimum for the minority channel.

The localized states that dominate the conductance in the minority channel at small thicknesses do not contribute as the semiconductor barrier layer thickness is increased. The current for the antialigned case has features of both the majority and minority currents for the aligned case. These results are quite different from those obtained[28] for tunneling through a simple step barrier that showed a current distribution that is peaked around the Γ point ($\mathbf{k}_\parallel = 0$). For this simple barrier, this is simply a consequence of the fact that the decay of states in the barrier region increases as $\mathbf{k}_\parallel$ increases.

In the case of a barrier formed from ZnSe, in addition to the decay in the barrier region, the coupling between states inside and outside the semiconductor is important. Thus, the peak in the conductance no longer need occur at the zone center. In the case of the majority electrons the decay within the barrier dominates, since the states close to Γ are able to couple efficiently with decaying states inside the barrier. Thus, the conductance is peaked around the zone center. In the case of the minority electrons states away from the zone center rather than those at $\mathbf{k}_\parallel = 0$ are able to tunnel more easily into the semiconductor layers. Thus, although these states would decay more rapidly than those at the zone center, they make the dominant contribution to the minority conductance. This net result is a very different current distribution compared to the majority conductance.

The differences in the decay rates seen in the conductance for majority and minority electrons, as well that seen for the antiparallel magnetic alignment, which are shown in Fig. 4 can be traced back to the symmetry of the Bloch states at the Fermi energy, and the correspondingly different spin injection/extraction efficiency for these bands between the Fe and the semiconductor. In Figs. 7, 8, and 9, the decay of the various Bloch states into the barrier are shown. The bands are labeled by the usual symmetry labels. There are four such bands for both spin channels, a doubly degenerate Δ_5 band (compatible with p and d symmetry), a $\Delta_{2'}$ (compatible with d symmetry) is seen for both majority and minority spins.
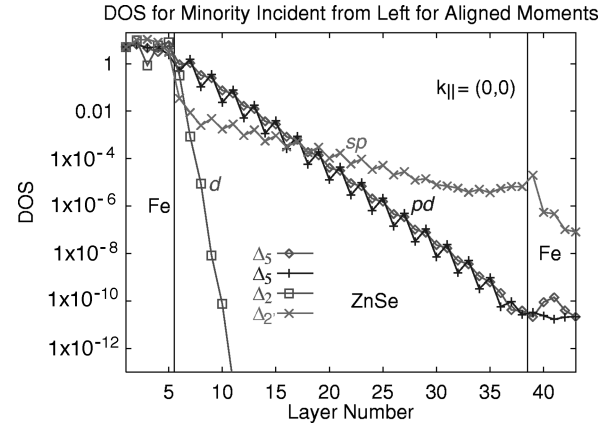
There is also a majority Δ_1 band (compatible with s, p, and d symmetry) and a minority band with Δ_2 symmetry (compatible with d symmetry). As can be seen in these figures, there are three decay rates, which are associated with the angular momentum character of the bands *within* the semiconductor barrier. The rate of decay is slowest for bands with s character and most rapid for those with only d character. In addition, to the different decay rates, the ease of injection and extraction is band dependent and depends upon the character of the band in the lead. In the majority channel, the Δ_1 band, because of the s character couples efficiently with a decaying sp state in the semiconductor, and thus, this band dominates the conductance. The $\Delta_{2'}$ majority band, because it is a pure d band in the bulk cannot couple efficiently with the sp state in the semiconductor. Thus we see that while the band decays slowly in the semiconductor, the coupling across the interface is weak. The doubly degenerate Δ_5 band couples to a pd decaying state in the semiconductor and as a consequence decays more rapidly in the barrier. In the case of the minority channel, similar arguments apply. The much smaller tunneling conductance seen is a direct result of there being no Δ_1 band present at the Fermi energy.

Based upon these results, certain general statements can be made. The expected spin dependence of the tunneling
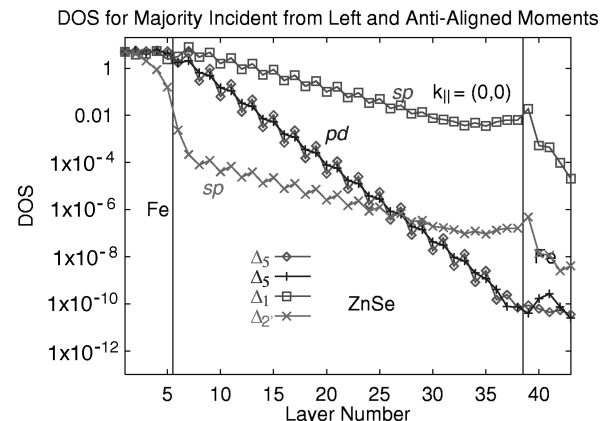
FIG. 9. Density of states for each of the Bloch states at $k_\parallel = 0$, for antiparallel alignment of the Fe moments. The left-hand side of the junction is spin up, while the right-hand side is spin down.

TABLE I. Type and symmetry of the Bloch states with $\mathbf{k}_\parallel = 0$ for Fe, Co, and Ni for three different crystal faces. The symmetry of these bands is as follows: Δ_1, Σ_1, and Λ_1 (s,p,d); Δ_5, and Σ_2 (p and d); and Δ_2, $\Delta_{2'}$, Σ_4, and $\Lambda_3(d)$.

	100	110	111
Fe↑	$\Delta_1, \Delta_{2'}, \Delta_5$	Σ_1, Σ_3	Λ_1
Fe↓	$\Delta_2, \Delta_{2'}, \Delta_5$	Σ_1, Σ_3	Λ_1
Co↑	Δ_1	Σ_1	
Co↓	Δ_1, Δ_5	Σ_2, Σ_4	
Ni↑	Δ_1	Σ_1, Σ_3	
Ni↓	$\Delta_1, \Delta_2, \Delta_5$	Σ_1, Σ_2	Λ_3

current can be deduced from the symmetry of the lead Bloch states at the Fermi energy. Those bands with s character are expected to be able to couple across the interface, and decay most slowly in the barrier. While bands without s character can also couple to decaying states with s character in the barrier, which then decay slowly, the poor coupling across the interface limits their contribution to the overall conductance. Thus, differences in the tunneling conductance will depend on both the substrate crystal face and the material. In the case of Fe, for example, an examination of the band structure shows that for [100], [111], and [110] directions all have majority bands with s character present, and for all but the [100] direction, a band with this symmetry also crosses the Fermi energy for the minority channel. Spin-polarized band structures for bcc Fe, fcc Ni, and fcc Co can be found in Ref. 30. Thus, based upon symmetry grounds, the [100] direction should exhibit the largest assymetry in tunnel conductance. Further, as a result of this we anticipate that only

Fe [100] based tunnel junctions would have an magnetoresistance (MR) that would increase with increasing barrier thickness. In the other growth directions, and in a polycrystalline film, the presence of states with s character for both spin directions would lead to states that decay at the same rate in barrier region, leading to an MR that would be thickness independent. The type and symmetry of the Bloch states with $\mathbf{k}_\parallel = 0$ for Fe, Co, and Ni are listed in Table I.

For Fe, Co, and Ni, the majority states at the Fermi energy are expected to have more s character than the minority states, which tend to be mainly d. Thus, the majority conductance is expected to be greater than the minority conductance. This is consistent with experimental data that also suggests this in the cases where it can be measured.[31] This is even the case for Ni where the minority density of states exceeds that at the Fermi energy by a factor of 10. Even though most of the tunnel junctions currently being studied are made from amorphous Al_2O_3, since the tunneling conductance is to a large part controlled by the symmetry of the lead Bloch states, we expect that these qualitative conclusions will be valid.

[1] R. Landauer, IBM J. Res. Dev. **1**, 223 (1957).

[2] J. M. MacLaren, S. Crampin, D. D. Vvedensky, R. C. Albers, and J. B. Pendry, Comput. Phys. Commun. **60**, 365 (1990).

[3] J. Barnaś, A. Fuss, R. E. Cameley, P. Grünberg, and W. Zinn, Phys. Rev. B **42**, 8110 (1990).

[4] R. Q. Hood and L. M. Falicov, Phys. Rev. B **46**, 8287 (1992); L. M. Falicov and R. Q. Hood, J. Appl. Phys. **76**, 6595 (1994).

[5] W. H. Butler, X.-G. Zhang, and J. M. MacLaren, IEEE Trans. Magn. **34**, 927 (1998).

[6] J. S. Moodera, L. R. Kinder, T. M. Wong, and R. Meservey, Phys. Rev. Lett. **74**, 3273 (1995).

[7] T. Miyazaki, T. Yaoi, and S. Ishio, J. Magn. Magn. Mater. **98**, L7 (1991); **126**, 430 (1993).

[8] T. Miyzaki and N. Tezuka, J. Magn. Magn. Mater. **139**, 4231 (1995).

[9] X. W. Li, Yu Lu, G. Q. Gong, Gang Xiao, A. Gupta, P. Lecoeur, J. Z. Sun, Y. Y. Wang, and V. P. Dravid, J. Appl. Phys. **81**, 5509 (1997).

[10] T. Kimura, Y. Tomioka, H. Kuwahara, A. Asamitsu, M. Tamura, and Y. Tokura, Science **274**, 1698 (1996).

[11] J. P. Perdew and Z. Zunger, Phys. Rev. B **23**, 5048 (1981).

[12] D. M. Ceperley and B. J. Adler, Phys. Rev. Lett. **45**, 566 (1980); D. M. Ceperley, Phys. Rev. B **18**, 3126 (1978).

[13] S. H. Vosko, K. Wilk, and M. Nusair, Can. J. Phys. **58**, 1200 (1989).

[14] J. M. MacLaren, S. Crampin, D. D. Vvedensky, and J. B. Pendry, Phys. Rev. B **40**, 12 164 (1989).

[15] W. H. Butler, X.-G. Zhang, D. M. C. Nicholson, and J. M. MacLaren, Phys. Rev. B **52**, 13 399 (1955).

[16] E. Anderson, Z. Bai, C. Bischof, J. Dongarra, J. Du Croz, A. Greenbaum, S. Hammarling, A. McKenney, S. Ostrouchov, and D. Sovrensen, *LAPACK User's Guide (Second Edition)*, (SIAM Publications, Philadelphia, 1995). Information concerning LAPACK can be found at URL: http://www.netlib.org/lapack/index.html.

[17] M. D. Stiles and D. R. Hammann, Phys. Rev. B **38**, 2021 (1988).

[18] M. D. Stiles and D. R. Hammann, Phys. Rev. B **41**, 5280 (1990).

[19] G. Wachutka and H. Bross, J. Phys. A **15**, 3083 (1982).

[20] G. Wachutka, Phys. Rev. B **34**, 8512 (1986).

[21] J. van Hoof, Ph.D. Thesis, Catholic University of Nijmegan, 1997.

[22] J. E. Inglesfield and G. A. Bensch, Phys. Rev. B **37**, 6682 (1988).

[23] W. H. Butler, X.-G. Zhang, X.-D. Wang, J. van Ek, and J. M. MacLaren, J. Appl. Phys. **81**, 5518 (1997).

[24] C. B. Duke, *Tunneling in Solids* (Academic, New York, 1969).

[25] R. Landauer, IBM J. Res. Dev. **1**, 223 (1957).

[26] M. Büttiker, IBM J. Res. Dev. **32**, 317 (1988).

[27] The issue of whether the conductance for a single channel is T or T/R is irrelevant here because R, the reflection probability, is essentially unity.

[28] J. M. MacLaren, X.-G. Zhang, and W. H. Butler, Phys. Rev. B

56, 11 827 (1997).

[29] J. C. Slonczewski, Phys. Rev. B **39**, 6995 (1989).

[30] V. L. Moruzzi, J. F. Janak, and A. R. Williams, *Calculated Electronic Properties of Metals* (Pergamon, New York, 1978).

[31] R. Meservey and P. M. Tedrow, Phys. Rep. **238**, 173 (1994).